
TARDIS: TIME ATTENUATED REPRESENTATION DISENTANGLEMENT FOR INCOMPLETE MULTI-MODAL TUMOR SEGMENTATION AND CLASSIFICATION

Zishuo Wan ^{*}, Qinqin Kang ^{*}, Yi Huang, Yun Bian [‡], Dawei Ding [‡], and Ke Yan [†]

ABSTRACT

Tumor segmentation and diagnosis in contrast-enhanced Computed Tomography (CT) rely heavily on the physiological dynamics of contrast agents. However, obtaining a complete multi-phase series is often clinically unfeasible due to radiation concerns or scanning limitations, leading to the "missing modality" problem. Existing deep learning approaches typically treat missing phases as absent independent channels, ignoring the inherent temporal continuity of hemodynamics. In this work, we propose Time Attenuated Representation Disentanglement (TARDIS), a novel physics-aware framework that redefines missing modalities as missing sample points on a continuous Time-Attenuation Curve. TARDIS explicitly disentangles the latent feature space into a time-invariant static component (anatomy) and a time-dependent dynamic component (perfusion). We achieve this via a dual-path architecture: a quantization-based path using a learnable embedding dictionary to extract consistent anatomical structures, and a probabilistic path using a Conditional Variational Autoencoder to model dynamic enhancement conditioned on the estimated scan time. This design allows the network to hallucinate missing hemodynamic features by sampling from the learned latent distribution. Extensive experiments on a large-scale private abdominal CT dataset (2,282 cases) and two public datasets demonstrate that TARDIS significantly outperforms state-of-the-art incomplete modality frameworks. Notably, our method maintains robust diagnostic performance even in extreme data-sparsity scenarios, highlighting its potential for reducing radiation exposure while maintaining diagnostic precision.

Keywords: Computed Tomography, Incomplete Modalities, Representation Disentanglement, Time-Attenuation Curve, Tumor Segmentation and Classification

1 Introduction

Tumor segmentation in contrast-enhanced Computed Tomography (CT) is fundamentally dependent on the transient physiological dynamics of the contrast agent [1]. Crucially, the diagnostic boundaries of tumors are often defined by this time-dependent contrast-enhancement signal, which is unavailable in non-contrast acquisitions or incorrectly timed scans [2]. Accurately capturing these dynamics usually requires a multi-phase acquisition protocol. However, obtaining a complete set of phases is not always feasible in clinical practice due to radiation dose concerns, patient motion, or limited scanning time. This creates a significant "missing modality" problem, where crucial enhancement information is absent, leading to severe degradation in segmentation performance for standard learning-based frameworks [3].

Existing approaches to multi-modal segmentation typically rely on channel-concatenation strategies, which assume a fixed set of inputs. When a modality is missing, these models often fail or require retraining. To address this, recent

¹Zishuo Wan and Qinqin Kang are co-first authors.

²Corresponding authors: Yun Bian, Dawei Ding, Ke Yan.

³Zishuo Wan, and Dawei Ding are with the School of Automation and Electrical Engineering, University of Science and Technology Beijing, Beijing 100083, China (e-mail: d202410372@xs.ustb.edu.cn; dingdawei@ustb.edu.cn).

⁴Yi Huang, and Ke Yan are with Alibaba Group DAMO Academy, Beijing 100026, China, and also with Hupan Lab, Hangzhou 310023, China (e-mail: yanke.yan@alibabinc.com).

⁵Qinqin Kang, and Yun Bian are with the Departments of Radiology, Changhai Hospital, Shanghai, China.

"incomplete modality" frameworks have been proposed, utilizing techniques such as arithmetic mean fusion, knowledge distillation, or shared latent space mapping [4, 5]. While these methods allow for flexible inputs, they generally treat different contrast phases as independent, uncorrelated channels or simple statistical variations. By ignoring the temporal dependency between phases, existing methods struggle to infer the missing dynamic information effectively, often resulting in suboptimal feature representation [6, 7].

In this work, we propose Time Attenuated Representation Disentanglement (TARDiS), a novel framework that addresses the incomplete modality challenge by modeling the underlying hemodynamics of CT. Our central hypothesis is that the Hounsfield Unit (HU) intensity can be explicitly decoupled into a time-invariant static component and a time-dependent dynamic component. Rather than treating missing modalities as empty data channels, we treat them as missing samples on the TAC. Our method employs a shared encoder to process a flexible number of input modalities. To learn robust representations, we introduce a dual-path disentanglement mechanism. First, we extract a modal-agnostic anatomical representation using a learnable embedding dictionary, ensuring consistency across different scans. Second, we model the modal-specific dynamic representation using a Conditional Variational Autoencoder (CVAE) [8], which is conditioned on the anatomy and the estimated scan time. This allows the network to probabilistically reconstruct the dynamic enhancement features of the tumor even when specific phases are missing. By explicitly disentangling anatomy from time-dependent perfusion, TARDiS learns a physically grounded latent space that is robust to missing data, superior to standard fusion or masking strategies.

2 Related Works

2.1 Multi-Modal Medical Image Segmentation

Multi-modal learning has become a cornerstone in medical image analysis, as combining complementary information from different modalities significantly improves diagnostic precision [9]. Early approaches focused on input-level fusion, where registered modalities are concatenated as multi-channel inputs to a Convolutional Neural Network [10, 11]. While effective, this assumes a fixed set of inputs, making the model fragile to missing data. Feature-level fusion strategies have subsequently emerged to better exploit cross-modal correlations. For instance, Dolz et al. [12] proposed HyperDenseNet to facilitate dense connectivity across multi-modal streams. More recently, Transformer-based architectures have been adopted to model long-range dependencies across modalities. Hatamizadeh et al. [13] introduced UNETR, which utilizes a vision transformer encoder to fuse volumetric data. Despite their success, these "complete-modality" frameworks rely on the assumption that all training and testing modalities are available. In clinical practice—particularly in multi-phase CT—scans are often incomplete due to radiation dose concerns or varying acquisition protocols, rendering these rigid fusion models ineffective without retraining or zero-filling strategies that often introduce artifacts.

2.2 Learning with Incomplete Modalities

To address the "missing modality" problem, recent research has shifted toward flexible frameworks capable of handling arbitrary subsets of inputs. The pioneering work of HeMIS [14] proposed learning a shared latent representation where first- and second-order statistics of available modalities are fused. This statistical fusion concept was extended by Dorent et al. [15] in the U-HVED framework, which integrates a multi-modal VAE to reconstruct missing inputs. Other approaches employ knowledge distillation (KD) to transfer information from a "complete-modality" teacher to an "incomplete-modality" student [16, 17]. However, KD methods typically require a complete set of modalities during the training phase, which may not always be available in retrospective cohorts. More recently, network architecture designs have moved toward adaptive feature fusion. RFNet [18] utilizes region-aware fusion to selectively aggregate features based on image content. With the rise of Transformers, methods like mmFormer [19] and M2FTrans [20] employ masked attention mechanisms to learn intra- and inter-modal correlations, effectively "masking out" missing tokens. M3AE [21] adapts the Masked Autoencoder (MAE) paradigm to multi-modal settings. While these methods achieve state-of-the-art results, they generally treat modalities as independent, uncorrelated channels.

2.3 Representation Disentanglement and Generative Modeling

Representation disentanglement aims to decompose data into distinct, explanatory factors, typically separating spatial structure from appearance. In natural image synthesis, methods like MUNIT [22] and DRIT++ [23] successfully disentangle content and style codes. In medical imaging, this paradigm has been applied to improve robustness and interpretability. Chartsias et al. [24] utilized disentanglement for synthesizing missing MRI sequences. SDNet [25] further decomposes medical images into spatial anatomy and non-spatial modality factors to improve segmentation generalization. VQ-VAE [26] demonstrates that quantizing latent features can effectively remove noise and preserve

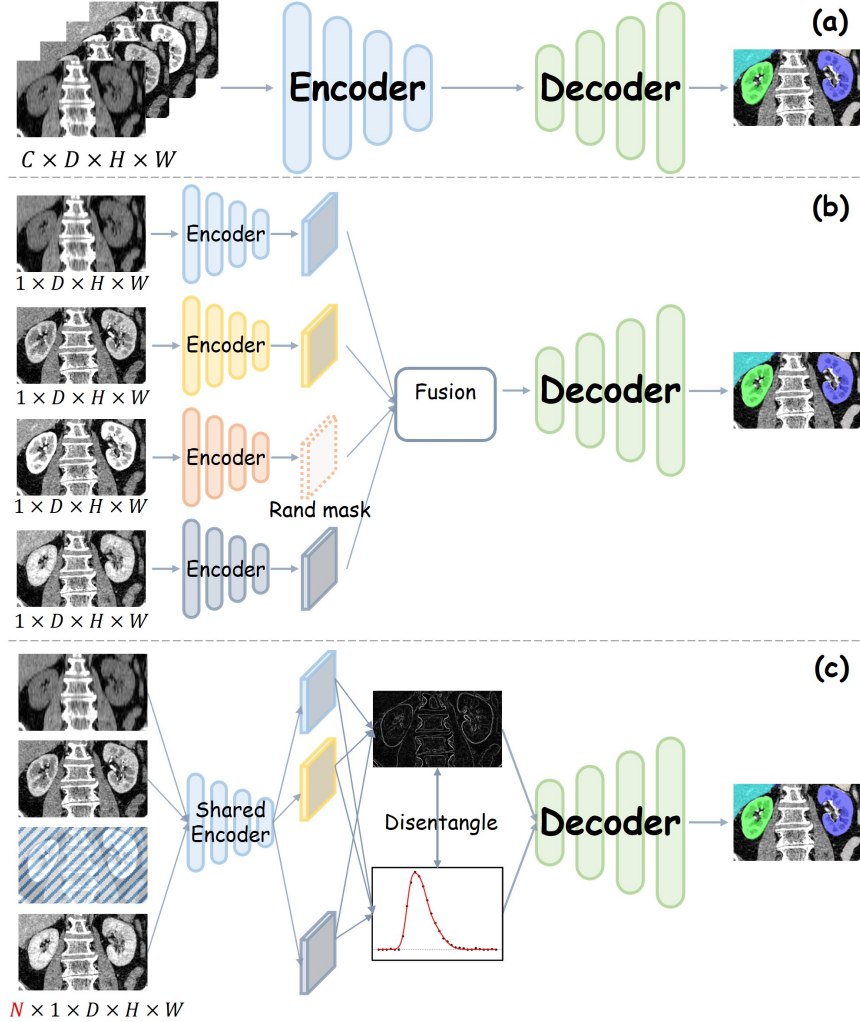


Figure 1: Comparison of segmentation frameworks. (a) Standard U-Net takes a fixed number of modalities. (b) Existing incomplete modality methods that use separate encoders for fixed modalities and fuse them by randomly masking. (c) Our proposed method TARDiS, which takes a flexible number of modalities (N), processes them via a shared encoder, and explicitly disentangles them into modal-agnostic (anatomic) and modal-specific (temporal) representations before decoding.

essential structural information. In the context of missing data, Generative Adversarial Networks and VAEs are often used to impute missing modalities before segmentation [27, 28]. However, most existing generative imputation methods perform image-to-image translation without explicit physical grounding.

3 Method

3.1 Problem Formulation

To address the challenges of incomplete modalities, we propose a method based on a decomposition of the Hounsfield Unit (HU) value. In multi-phase CT, the HU value at any spatial location $\mathbf{p} = (z, x, y)$ is a function of the time τ elapsed since the injection of a contrast agent. This function, $H(\mathbf{p}, \tau)$, is known as the Time-Attenuation Curve (TAC) and describes the complete perfusion profile of the tissue at that location, as shown in Fig. 2. Clinically, a *modality* (e.g., Arterial, Venous, Delayed phase) corresponds to a single sample of this curve at a specific time τ . A non-contrast CT represents the baseline at $\tau = 0$.

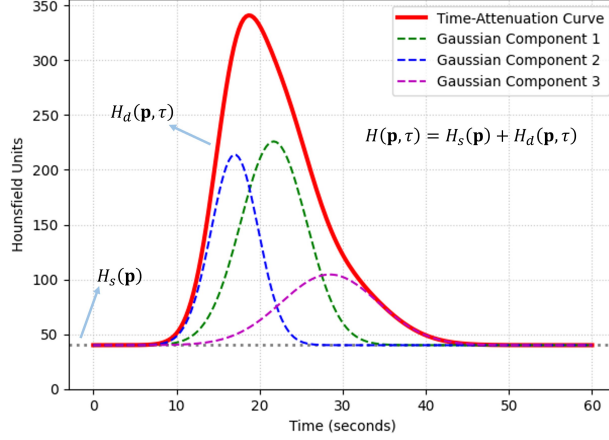


Figure 2: The Time-Attenuation Curve of a certain spatial location \mathbf{p} in a CT volume. The static component $H_s(\mathbf{p})$ is related to the tissue’s natural density. And the dynamic component $H_d(\mathbf{p}, \tau)$ reflects how the Hounsfield Unit changes as the contrast agent passes the tissue, which can be approximated with several Gaussian distributions.

Our central hypothesis is that the TAC can be explicitly disentangled into two components: a static component $H_s(\mathbf{p})$ and a dynamic component $H_d(\mathbf{p}, \tau)$, which can be formulated as:

$$H(\mathbf{p}, \tau) = H_s(\mathbf{p}) + H_d(\mathbf{p}, \tau). \quad (1)$$

Here, $H_s(\mathbf{p})$ is the time-invariant static component, which reflects the intrinsic anatomical properties and base density of the tissue at location \mathbf{p} . It is equivalent to the non-contrast value, $H_s(\mathbf{p}) = H(\mathbf{p}, 0)$. Since this anatomical information is shared across all phases, we treat it as the modal-agnostic representation. Conversely, $H_d(\mathbf{p}, \tau)$ is the time-dependent dynamic component. It captures the enhancement profile as the contrast agent perfuses the tissue. This component is, by definition, modal-specific, as it dictates the unique appearance of each contrast phase.

Based on this physical decomposition, our computational goal is to learn a disentangled latent representation for a given position \mathbf{p} that separates its static properties from its dynamic properties. We propose a model that learns to map multi-modal input CT volumes I_N to a pair of latent representations:

1. A modal-agnostic representation X_s , which is discrete and aims to capture the intrinsic, time-invariant anatomical properties analogous to $H_s(\mathbf{p})$.
2. A modal-specific representation X_d , which is continuous and probabilistic, aiming to capture the time-dependent enhancement profile analogous to $H_d(\mathbf{p}, \tau)$.

We further hypothesize that the dynamic enhancement profile H_d is conditional on the underlying anatomical properties H_s :

$$H_d(\mathbf{p}, \tau) \sim q(H_s(\mathbf{p}), \tau). \quad (2)$$

Therefore, TARDiS is designed such that the generation of the modal-specific representation X_d is explicitly conditioned on the modal-agnostic representation X_s and the phase time τ . The final, disentangled representation $X = \{X_s, X_d\}$ is then used for the downstream segmentation task. The details will be given in the following sections.

3.2 Overall Architecture

The overall architecture of TARDiS is illustrated in Fig. 3(a). Unlike previous incomplete modality methods that use separate encoders for fixed inputs, we employ a shared encoder to extract features from a flexible number of modalities. When taking a series of registered incomplete multi-modal CT volumes I_N as inputs, each of the input modality volumes $I_i \in \mathbb{R}^{1 \times D \times H \times W}$, $i \in \{1, 2, \dots, N\}$ is independently processed by a shared 3D encoder, producing a feature map $F_i \in \mathbb{R}^{C \times D' \times H' \times W'}$. These multi-modal features are then disentangled by a pair of projectors and flattened into sequences of tokens $X_s \in \mathbb{R}^{N \times C \times K}$ and $X_d \in \mathbb{R}^{N \times C \times K}$. Then the tokens are processed by two distinct paths. The modal-agnostic path extracts a common static anatomical representation $\hat{X}_s \in \mathbb{R}^{C \times K}$ using a shared embedding dictionary (Sec. 3.3). The modal-specific path estimates the phase time τ_i and uses a CVAE to model and sample the dynamic representations $\hat{X}_d \in \mathbb{R}^{N \times C \times K}$ for all modalities (Sec. 3.4). The derived anatomic representation and the multi-modal dynamic representations are adaptively assembled (Sec. 3.5), reshaped back to spatial dimensions, and

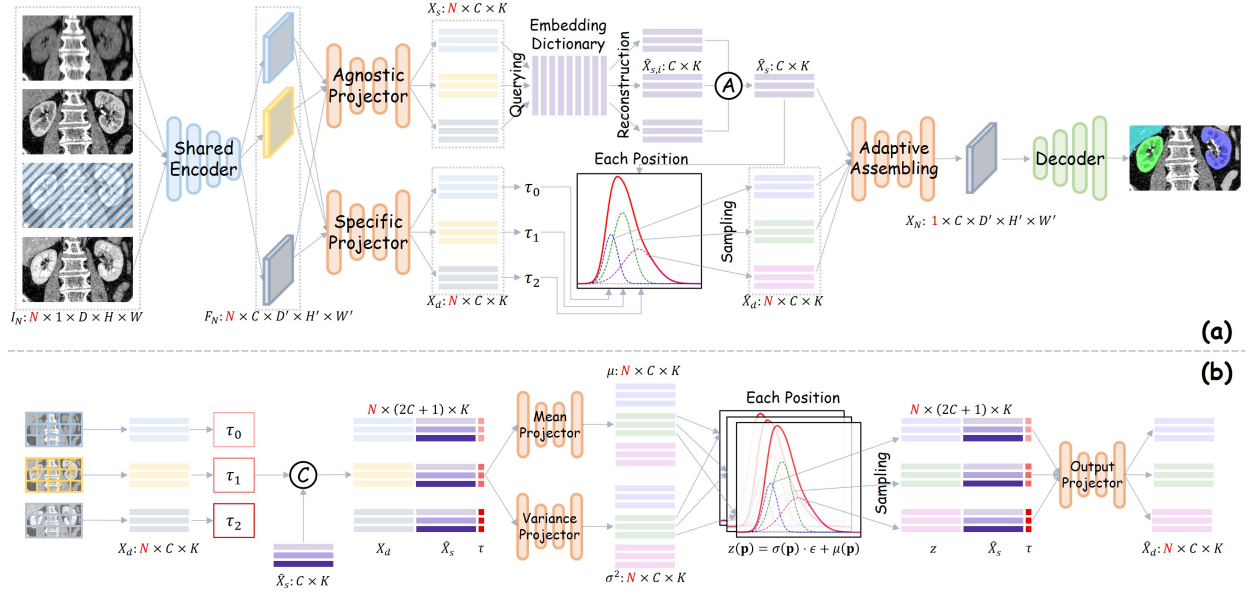


Figure 3: (a) The overall architecture of TARDiS. Input volumes are processed by a shared encoder. The features are projected and flattened into K tokens. The modal-agnostic path (top) queries an embedding dictionary to extract consistent anatomic features. The modal-specific path (bottom) regresses a relative time τ and uses a Conditional Variational Autoencoder (CVAE) conditioned on the average anatomy and τ to sample dynamic features. Finally, the aggregated representations are assembled and decoded by a U-Net decoder. (b) The detailed workflow of the modal-specific path. Every token $X_{d,i}(\mathbf{p})$ contains the dynamic features of a neighboring subregion in different modalities. First, a τ_i is regressed based on dynamic features. Then we treat the time τ_i and modal-agnostic anatomic features $\hat{X}_s(\mathbf{p})$ as the conditions, and project the dynamic features of each position \mathbf{p} into Gaussian means $\mu(\mathbf{p})$ and variances $\sigma^2(\mathbf{p})$. Then we reparameterize the tokens with $\epsilon(\mathbf{p}) \in \mathcal{N}(0, I)$ and reconstruct the $\hat{X}_{d,i}(\mathbf{p})$. When inferring, we can sample $z(\mathbf{p})$ directly from $\mathcal{N}(0, I)$ and generate the corresponding dynamic representations with respect to the given $(\hat{X}_s(\mathbf{p}), \tau_i)$.

passed to a decoder to predict the final segmentation mask. The entire network is trained jointly using the objectives detailed in Sec. 3.6.

3.3 Modal-Agnostic Representations

The static component represents the inherent anatomy, which should be consistent across all phases. However, features extracted from different contrast phases often contain phase-specific noise that obscures this underlying anatomy. Inspired by VQ-VAE [26], we construct a discrete learnable Embedding Dictionary $\mathcal{D} \in \mathbb{R}^{M \times C}$, containing M anatomical vision queries, into which the anatomical information is distilled by quantization.

For each input modality i , the projected static feature at any position $X_{s,i}(\mathbf{p}_k) \in \mathbb{R}^{C \times K}$ is used to find the nearest query in the dictionary, and reconstructed by the discrete queries:

$$\hat{X}_{s,i}(\mathbf{p}_k) = q_k, \quad k = \underset{q_j \in \mathcal{D}}{\operatorname{argmin}} \|X_{s,i}(\mathbf{p}_k) - q_j\|_2 \quad (3)$$

where $k \in \{1, 2, \dots, K-1\}$. This process reconstructs a refined multi-modal feature $\hat{X}_{s,N}$ by aggregating relevant queries from \mathcal{D} . To constrain the consistency of the anatomical information in multi-modal representations, we introduce pair-wise mean squared loss to the querying results:

$$\mathcal{L}_{\text{Consis}} = \sum_{i \neq j} (\hat{X}_{s,i}(\mathbf{p}) - \hat{X}_{s,j}(\mathbf{p}))^2. \quad (4)$$

This constrains the individual embeddings $\hat{X}_{s,i}$ from different phases to be close to this global average (and thus to each other), regardless of the input modality. This explicitly aligns the latent spaces of different phases into a unified

anatomical space. By constraining, the reconstructed features $\hat{X}_{s,i}$ should be identical for all $i \in \{1, 2, \dots, N\}$. To enforce this, we compute the mean of these reconstructed features to obtain a robust, global anatomic representation:

$$\hat{X}_s(\mathbf{p}) = \frac{1}{N} \sum_{i=1}^N \hat{X}_{s,i}(\mathbf{p}), \quad (5)$$

which is also considered as the conditional information to construct dynamic information. The overall loss of the modal-agnostic path can be written as:

$$\mathcal{L}_{\text{Agn}} = \mathcal{L}_{\text{Consis}} + \|\text{sg}[\hat{X}_{s,i}] - X_{s,i}\|_2^2 + \beta \|\hat{X}_{s,i} - \text{sg}[X_{s,i}]\|_2^2, \quad (6)$$

where $\text{sg}[\cdot]$ means stop gradient.

3.4 Sampling Based Modal-Specific Representations

The dynamic component varies significantly with time, reflecting the perfusion of contrast agents. To model this complex, time-dependent distribution, we design a generative module based on a CVAE. The details are shown in Fig. 3(b). This allows us to sample specific representations conditioned on the underlying anatomy and the particular time point.

We first must estimate where the current scan lies on the TAC curve, as the exact acquisition time is often unknown. We regress a relative time scalar τ_i directly from the modal-specific feature $X_{d,i}$ using a lightweight regressor network \mathcal{R} :

$$\tau_i = \mathcal{R}(X_{d,i}) \in [0, 1], \quad (7)$$

under the constraint of a Margin Ranking Loss:

$$\mathcal{L}_{\text{Rank}} = \frac{1}{|\mathcal{P}_k|} \sum_{(j,i) \in \mathcal{P}_k} \max(0, \tau_i - \tau_j + m), \quad (8)$$

where m is the margin, and $\mathcal{P}_k = \{(j, i) \mid j > i, j, i \in \{1, 2, \dots, N\}\}$. This relative time serves as a critical condition for the generative process, signaling the phase of the contrast enhancement.

We model the distribution of continuous latent representations using a CVAE. The core idea is that dynamic enhancement is a function of both tissue type and time. Therefore, the generation of a specific dynamic feature $\hat{X}_d(\mathbf{p})$ at any position \mathbf{p} is conditioned on two variables: the neighboring anatomic representation $\hat{X}_s(\mathbf{p})$, which provides the structural context, and the relative time τ_i , which provides the phase context.

The CVAE's objective is to learn a probabilistic mapping for the dynamic features, which consists of an encoder and a decoder. The encoder q_ψ approximates the posterior Gaussian distribution $p(z(\mathbf{p})|X_d(\mathbf{p}), \hat{X}_s(\mathbf{p}), \tau)$:

$$\begin{aligned} z(\mathbf{p}) &\sim q_\psi(z(\mathbf{p})|X_d(\mathbf{p}), \hat{X}_s(\mathbf{p}), \tau) \\ &= \mathcal{N}(z(\mathbf{p}); \mu_\psi(\mathbf{p}), \sigma_\psi^2(\mathbf{p})I), \end{aligned} \quad (9)$$

by predicting its mean and variance:

$$\begin{aligned} \mu_\psi(\mathbf{p}) &= \mu_\psi(X_d(\mathbf{p}), \hat{X}_s(\mathbf{p}), \tau) \\ \sigma_\psi^2(\mathbf{p}) &= \sigma_\psi^2(X_d(\mathbf{p}), \hat{X}_s(\mathbf{p}), \tau). \end{aligned} \quad (10)$$

The decoder p_θ then reconstructs the original dynamic feature for each modality $\hat{X}_{d,i}(\mathbf{p})$ from the sampled and reparameterized latent variable z and the respective conditions $\mathbf{c}_i(\mathbf{p}) = (\hat{X}_s(\mathbf{p}), \tau_i)$:

$$\hat{X}_{d,i}(\mathbf{p}) = p_\theta(X_{d,i}(\mathbf{p})|z_i(\mathbf{p}), \mathbf{c}_i(\mathbf{p})). \quad (11)$$

During training, this CVAE module is trained with KL Divergence and reconstruction loss. The total loss of the modal-specific path is:

$$\begin{aligned} \mathcal{L}_{\text{Spe}} &= \mathcal{L}_{\text{Rank}} + \underbrace{\mathbb{E}_{q_\psi}[-\log p_\theta(X_d|z, \mathbf{c})]}_{\text{Reconstruction Loss}} \\ &\quad + \lambda \underbrace{D_{KL}(q_\psi(z|X_d, \mathbf{c})\|p_\theta(z|\mathbf{c}))}_{\text{KL Divergence}} \end{aligned} \quad (12)$$

where $p_\theta(z|\mathbf{c})$ is the conditional prior, which is a centered isotropic multivariate Gaussian $p_\theta(z|\mathbf{c}) = \mathcal{N}(z; 0, I)$.

Crucially, the CVAE is conditioned on the output of the modal-agnostic module and the known phase. This aligns with our physical model where the dynamic enhancement H_d depends on the static tissue H_s and time τ in Eq. (2). By training this CVAE, it is capable of capturing the dynamic enhancement properties at position \mathbf{p} for a specific phase τ . This generative design provides a powerful mechanism for handling missing modalities. For flexible input modalities in the inference stage, a relative time τ_i can be predicted for each modality. And then a corresponding dynamic representation $\hat{X}_{d,i}$ can be generated by sampling equivalent z_i from the prior distribution and decoding it with the inferred anatomy \hat{X}_s and the target time τ_i .

3.5 Adaptive Assembly

The disentangled representations $\hat{X}_s \in \mathbb{R}^{C \times K}$ and $\hat{X}_d \in \mathbb{R}^{N \times C \times K}$ capture complementary information. Because of the uncertainty of N , the representations cannot be simply concatenated and sent into the fixed-channel decoder. Moreover, their relative importance for the final segmentation task might vary.

We therefore propose an adaptive assembling module that learns to optimally weight and combine the representations. This module is implemented with an attention mechanism, which computes the attention weights at each position \mathbf{p} . For the static and dynamic representations for all modalities $\hat{X}_m = \{\hat{X}_s, \hat{X}_d\}$, $m \in \{1, 2, \dots, N+1\}$, we calculate the attention score with:

$$\alpha_m(\mathbf{p}) = \text{Softmax}_m(\text{FFN}(\hat{X}_m(\mathbf{p}))) \quad (13)$$

where FFN means a shared small feed-forward network. This FFN regresses an importance score for each representation at \mathbf{p} . And then the importance scores are normalized as the attention weights. It's worth noting that the attention weights can vary at different positions, which enables the model to decide which modality to focus on when classifying a certain voxel. The final fused representation $\hat{X}(\mathbf{p})$ is a weighted sum:

$$X_N(\mathbf{p}) = \sum_{m=1}^{N+1} \alpha_m(\mathbf{p}) \hat{X}_m(\mathbf{p}). \quad (14)$$

This $X_N \in \mathbb{R}^{1 \times C \times K}$ is then reshaped as F_N and passed to a segmentation decoder to produce the final mask.

3.6 Optimization Objectives

The entire model is trained end-to-end by optimizing a composite loss function $\mathcal{L}_{\text{total}}$, which is a weighted sum of four components:

$$\mathcal{L}_{\text{total}} = \mathcal{L}_{\text{Agn}} + \mathcal{L}_{\text{Spe}} + \mathcal{L}_{\text{DE}} + \mathcal{L}_{\text{Seg}}, \quad (15)$$

where \mathcal{L}_{DE} is the disentanglement loss and \mathcal{L}_{Seg} is the segmentation loss. Following [29], we use CLUB loss [30] to disentangle the representations by mutual information (MI) minimization, which provides a contrastive upper bound on MI, preventing information leakage between the anatomical and temporal latent spaces. Specifically, we calculate

$$\mathcal{L}_{\text{DE}} = \sum_{i \neq j} \mathcal{L}_{\text{CLUB}}(\hat{X}_{m,i}, \hat{X}_{m,j}) \quad (16)$$

to minimize the MI not only between the static and dynamic representations, but also among multi-modal dynamic representations. \mathcal{L}_{Seg} is the primary task loss, driving the final segmentation. We use a standard combination of Dice and Cross-Entropy (CE) loss:

$$\mathcal{L}_{\text{Seg}} = \mathcal{L}_{\text{Dice}}(S, \hat{S}) + \mathcal{L}_{\text{CE}}(S, \hat{S}) \quad (17)$$

where S and \hat{S} are the ground-truth and predicted segmentation masks, respectively.

3.7 Handling Variable Modality Sequences

A core strength of TARDIS is its ability to process an arbitrary number of input modalities N , where N varies across different patients and clinical scenarios. This variability presents challenges for standard batch-based optimization. We address this through a sequence-based training strategy and specific inference protocols. The variance of N is taken into consideration in every part of training and inference, including data loading, representation encoding, multi-modal assembly (Sec. 3.5), and loss calculation.

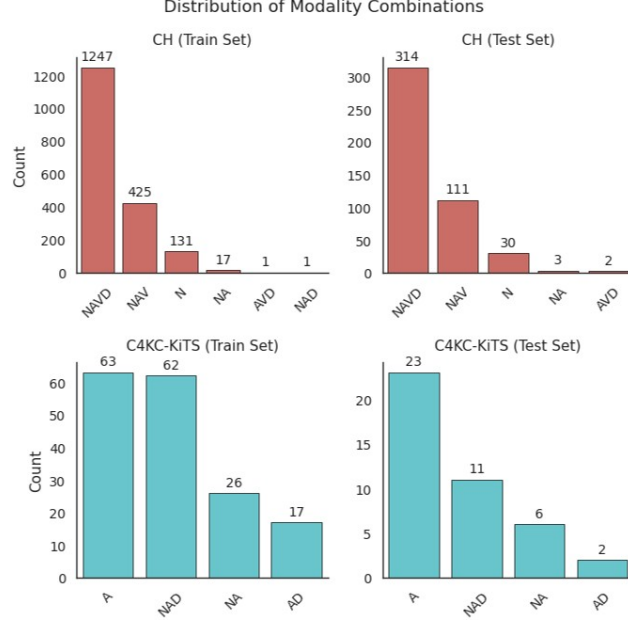


Figure 4: The distribution of modality combinations in CT datasets. N: Non-Contrast Scan. A: Arterial Phase. V: Portal Venous Phase. D: Delayed Phase. CH: ChangHai Dataset. KiTS19: Kidney Tumor Segmentation 2019 Dataset.

Sequence-Based Optimization

In standard deep learning frameworks, input tensors typically require fixed dimensions across a batch. Since our input is a set of volumes I_N where N is variable, we treat the input batch as a collection of independent sequences rather than a rigid tensor. Let a training batch \mathcal{B} consist of B subjects, where the b -th subject possesses N_b modalities. The total loss is computed by aggregating sample-wise losses, normalized by the sequence length of each subject:

$$\mathcal{L}_{batch} = \frac{1}{B} \sum_{b=1}^B \left(\frac{1}{\omega(N_b)} \mathcal{L}_{total}^{(b)} \right), \quad (18)$$

where $\omega(N_b)$ is a normalization factor accounting for the combinatorial number of pairs in the consistency, ranking, and CLUB losses (Eq. 4,8,16). This ensures that subjects with more available modalities do not dominate the gradient updates.

Modality Dropout

To simulate the "missing modality" problem explicitly during training, we employ an aggressive *Modality Dropout* strategy. Given a subject with a complete set of multi-phase acquisitions, we randomly subset the inputs to a smaller size $N' \leq N$ before passing them to the shared encoder. This stochastic dropping prevents the model from relying on any specific combination of phases and forces the shared encoder to extract robust anatomical features from sparse temporal samples.

Generative Inference

During inference, the model adapts to the specific subset of available modalities without architectural modification. For the modal-agnostic path, available inputs are encoded and queried against the dictionary to form \hat{X}_s . For the modal-specific path, we leverage the generative nature of the CVAE. The latent variables $z(p)$ are sampled directly from the prior distribution $\mathcal{N}(0, I)$. These are then decoded, conditioned on the inferred anatomy \hat{X}_s and the estimated relative time τ , to reconstruct the probabilistic dynamic representations \hat{X}_d . This allows TARDIS to understand the grounding of the tumor even in cases of extreme data sparsity (e.g., $N = 1$).

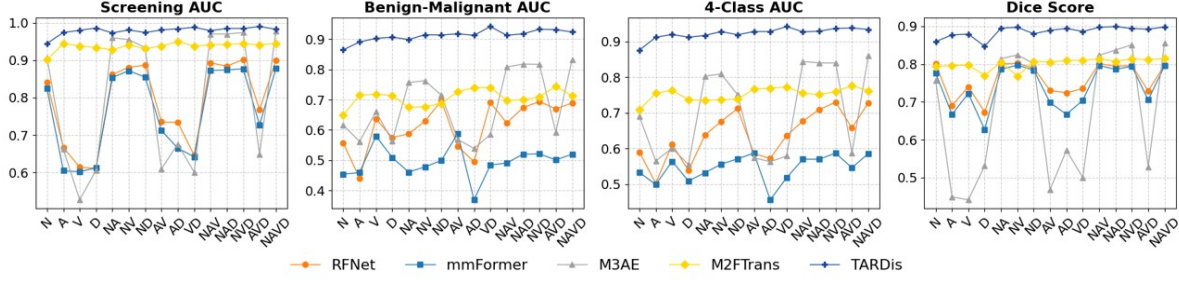


Figure 5: The metrics curves of comparison methods with different modality combinations in CH dataset. N: Non-Contrast Scan. A: Arterial Phase. V: Portal Venous Phase. D: Delayed Phase.

Table 1: Classification performance for tumor screening, benign-malignant classification, and diagnosis in CH dataset

Modality					Screening AUC					Benign-Malignant AUC					4-Class Diagnosis AUC				
N	A	V	D		[18]	[19]	[21]	[20]	TARDiS	[18]	[19]	[21]	[20]	TARDiS	[18]	[19]	[21]	[20]	TARDiS
✓					0.841	0.825	0.907	0.901	0.945	0.557	0.454	0.616	0.649	0.865	0.590	0.533	0.690	0.708	0.876
	✓				0.667	0.605	0.662	0.945	0.974	0.441	0.459	0.562	0.715	0.891	0.502	0.499	0.565	0.755	0.912
		✓			0.614	0.602	0.527	0.938	0.980	0.637	0.580	0.660	0.718	0.903	0.612	0.564	0.601	0.763	0.920
			✓		0.611	0.613	0.606	0.934	0.986	0.575	0.509	0.564	0.714	0.907	0.538	0.509	0.555	0.737	0.912
✓	✓				0.862	0.854	0.960	0.928	0.973	0.587	0.461	0.757	0.675	0.899	0.637	0.532	0.803	0.735	0.917
✓		✓			0.881	0.872	0.955	0.941	0.981	0.629	0.478	0.763	0.677	0.915	0.676	0.556	0.809	0.737	0.928
✓			✓		0.887	0.855	0.934	0.931	0.974	0.697	0.499	0.715	0.688	0.914	0.712	0.571	0.751	0.738	0.919
	✓	✓			0.735	0.712	0.610	0.938	0.981	0.546	0.588	0.569	0.727	0.918	0.586	0.587	0.574	0.767	0.928
	✓		✓		0.734	0.665	0.676	0.950	0.984	0.495	0.369	0.539	0.740	0.913	0.572	0.456	0.563	0.769	0.928
		✓	✓		0.646	0.642	0.601	0.938	0.988	0.691	0.484	0.585	0.741	0.942	0.636	0.518	0.579	0.773	0.942
✓	✓	✓			0.893	0.873	0.970	0.941	0.979	0.623	0.491	0.808	0.698	0.913	0.677	0.570	0.844	0.755	0.927
✓	✓		✓		0.884	0.874	0.970	0.943	0.985	0.674	0.520	0.818	0.700	0.918	0.709	0.570	0.840	0.751	0.929
✓		✓	✓		0.902	0.877	0.974	0.944	0.985	0.694	0.521	0.817	0.710	0.933	0.730	0.587	0.840	0.760	0.937
✓	✓	✓			0.768	0.727	0.648	0.941	0.990	0.670	0.501	0.593	0.744	0.932	0.658	0.546	0.587	0.776	0.938
✓	✓	✓	✓		0.900	0.878	0.979	0.945	0.983	0.689	0.520	0.833	0.713	0.924	0.728	0.586	0.860	0.762	0.934
Average					0.788	0.765	0.799	0.937	0.979	0.614	0.496	0.680	0.707	0.912	0.638	0.546	0.697	0.752	0.923

4 Results

4.1 Datasets

To evaluate the efficacy and robustness of TARDiS, we utilized three datasets comprising both Computed Tomography (CT) and Magnetic Resonance Imaging (MRI) modalities. The distribution of modality combinations for the CT datasets is illustrated in Fig. 4.

C4KC-KiTS

The first dataset is the *Climb 4 Kidney Cancer - Kidney and Kidney Tumor Segmentation* (C4KC-KiTS) collection [31, 32, 33], a public subset of the KiTS19 challenge data. We utilized 210 cases from the training set. As shown in Fig. 4, every case includes an arterial phase scan, while a subset of cases also contains non-contrast or delayed phase acquisitions, providing a controlled environment for testing missing-modality performance.

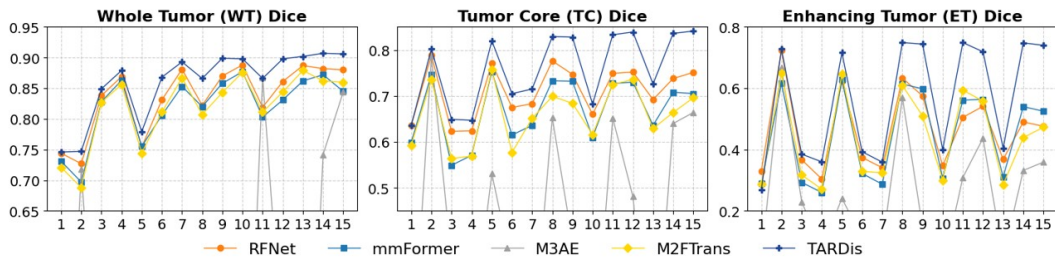


Figure 6: The metrics curves of comparison methods with different modality combinations in the BraTS18 dataset. The number on the x-axis refers to the modality combination in Table 4.

Table 2: Tumor segmentation performance in CH dataset

Modality				Segmentation Dice				
N	A	V	D	[18]	[19]	[21]	[20]	TARDis
✓				0.801	0.776	0.757	0.793	0.859
	✓			0.690	0.667	0.449	0.796	0.877
		✓		0.740	0.722	0.441	0.797	0.879
			✓	0.673	0.627	0.531	0.770	0.847
✓	✓			0.800	0.786	0.814	0.805	0.895
✓		✓		0.802	0.797	0.824	0.768	0.897
✓			✓	0.789	0.784	0.801	0.807	0.880
	✓	✓		0.730	0.698	0.468	0.805	0.889
	✓		✓	0.724	0.667	0.572	0.810	0.894
		✓	✓	0.735	0.704	0.500	0.809	0.886
✓	✓	✓		0.801	0.796	0.823	0.814	0.897
✓	✓		✓	0.794	0.786	0.837	0.807	0.899
✓		✓	✓	0.796	0.794	0.851	0.814	0.894
	✓	✓	✓	0.729	0.705	0.528	0.811	0.892
✓	✓	✓	✓	0.797	0.795	0.856	0.815	0.898
Average				0.760	0.740	0.670	0.801	0.885

Table 3: Segmentation and screening performance in KiTS19 dataset

Method	Segmentation			Screening		
	Dice	Precision	Recall	ACC	SEN	AUC
[18]	0.767	0.811	0.835	0.904	0.909	0.933
[19]	0.703	0.787	0.774	0.855	0.886	0.902
[21]	0.790	0.840	0.836	0.940	0.955	0.948
[20]	0.321	0.394	0.675	0.735	0.682	0.773
TARDis	0.825	0.860	0.841	0.952	0.955	0.965

Changhai (CH) Dataset

To validate our method in a large-scale clinical setting, we collected a private multi-phase abdominal CT dataset from Changhai Hospital, Shanghai, China. This extensive cohort contains 2,282 cases comprising 8,065 total scans (Fig. 4). The dataset includes 2,958 annotated kidney lesions spanning 26 distinct histological subtypes. For experimental purposes, these subtypes were categorized into four clinically relevant classes based on surgical management strategies: cysts (2,188), other benign lesions (105), low-grade malignant lesions (450), and high-grade malignant lesions (215).

Table 4: Tumor segmentation performance in BraTS18 dataset

Modality				Whole Tumor Dice					Tumor Core Dice					Enhancing Tumor Dice				
T1	T1CE	T2	FLAIR	[18]	[19]	[21]	[20]	TARDis	[18]	[19]	[21]	[20]	TARDis	[18]	[19]	[21]	[20]	TARDis
✓				0.744	0.731	0.045	0.721	0.746	0.636	0.599	0.056	0.593	0.636	0.330	0.289	0.043	0.287	0.269
	✓			0.727	0.697	0.718	0.688	0.747	0.788	0.746	0.787	0.735	0.802	0.723	0.616	0.668	0.650	0.728
		✓		0.838	0.828	0.223	0.827	0.849	0.623	0.549	0.341	0.564	0.649	0.367	0.293	0.230	0.317	0.385
			✓	0.869	0.863	0.136	0.856	0.879	0.624	0.571	0.175	0.569	0.647	0.304	0.260	0.076	0.271	0.360
✓	✓			0.754	0.755	0.624	0.744	0.779	0.771	0.753	0.531	0.757	0.820	0.623	0.628	0.241	0.646	0.716
✓		✓		0.831	0.806	0.451	0.811	0.868	0.675	0.615	0.323	0.577	0.705	0.374	0.322	0.111	0.329	0.393
✓			✓	0.881	0.853	0.082	0.867	0.893	0.683	0.636	0.143	0.651	0.715	0.341	0.287	0.083	0.324	0.359
	✓	✓		0.822	0.820	0.636	0.807	0.866	0.776	0.733	0.653	0.699	0.829	0.633	0.614	0.570	0.609	0.749
	✓		✓	0.870	0.858	0.498	0.843	0.899	0.747	0.732	0.382	0.684	0.828	0.575	0.598	0.147	0.510	0.744
		✓	✓	0.888	0.877	0.081	0.876	0.898	0.660	0.610	0.071	0.616	0.682	0.347	0.307	0.010	0.300	0.400
✓	✓	✓		0.819	0.803	0.868	0.811	0.866	0.749	0.727	0.652	0.725	0.833	0.505	0.561	0.309	0.594	0.749
✓	✓		✓	0.861	0.831	0.411	0.844	0.898	0.752	0.730	0.481	0.736	0.839	0.541	0.564	0.437	0.558	0.719
✓		✓	✓	0.887	0.862	0.041	0.879	0.902	0.692	0.636	0.053	0.629	0.726	0.368	0.311	0.050	0.286	0.405
	✓	✓	✓	0.882	0.872	0.742	0.862	0.907	0.738	0.708	0.640	0.664	0.836	0.490	0.540	0.332	0.439	0.748
✓	✓	✓	✓	0.880	0.845	0.844	0.860	0.906	0.751	0.705	0.664	0.696	0.841	0.476	0.525	0.359	0.473	0.740
Average				0.837	0.820	0.427	0.820	0.860	0.711	0.670	0.397	0.660	0.759	0.466	0.448	0.244	0.439	0.564

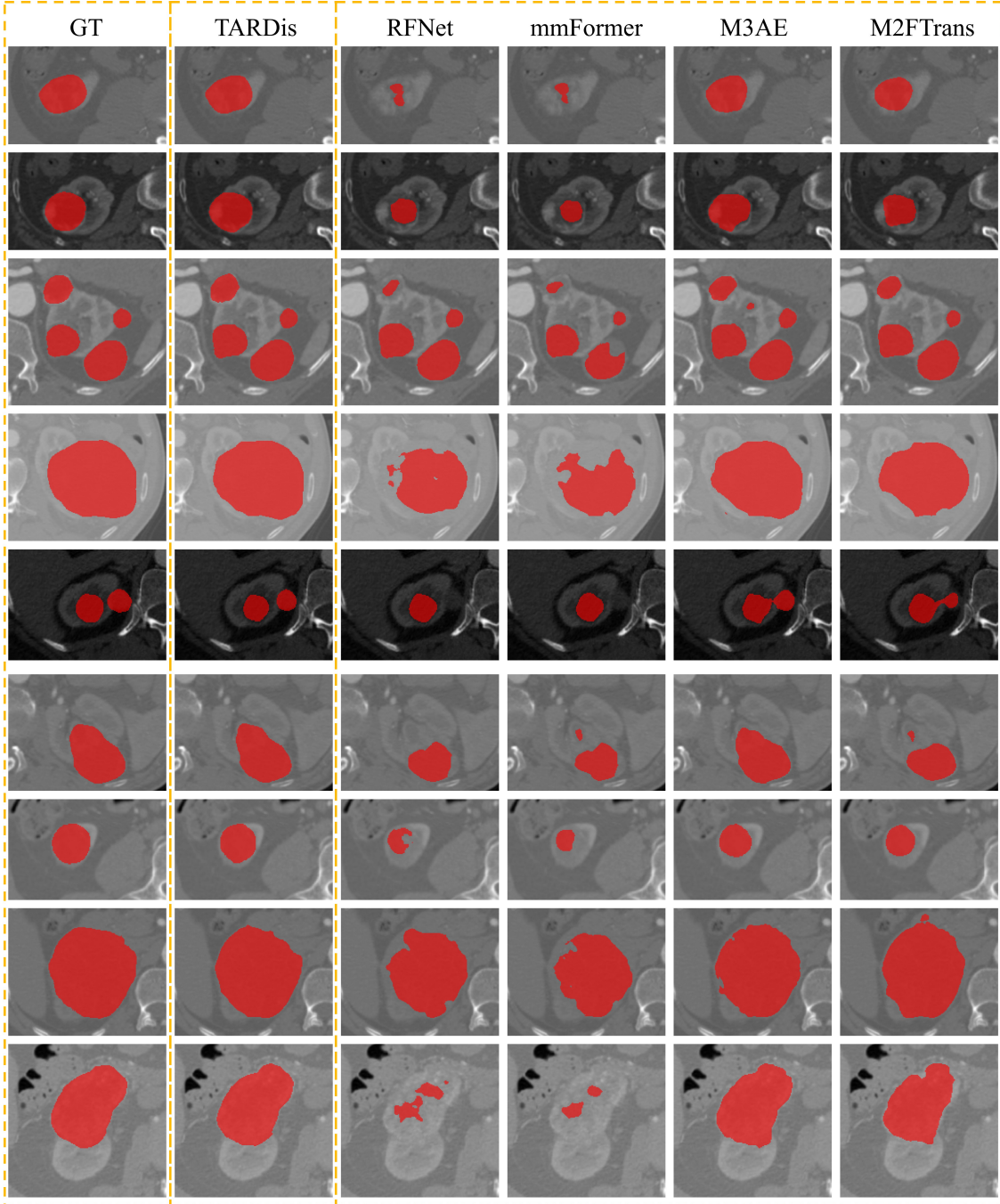


Figure 7: Qualitative comparison results for kidney tumor segmentation.

All volumes were spatially registered and preprocessed to facilitate multi-modal tumor diagnosis. Ground truth labels were annotated and iteratively refined by board-certified radiologists.

BraTS 2018

While TARDis is theoretically grounded in the CT modalities, we extended our evaluation to the BraTS 2018 dataset [34, 35, 36] to benchmark against existing state-of-the-art (SOTA) incomplete modality frameworks, which are predominantly established on this neuroimaging standard. BraTS18 provides four co-registered MRI modalities per case: T1-weighted (T1), post-contrast T1-weighted (T1CE), T2-weighted (T2), and FLAIR. Annotations include three nested sub-regions:

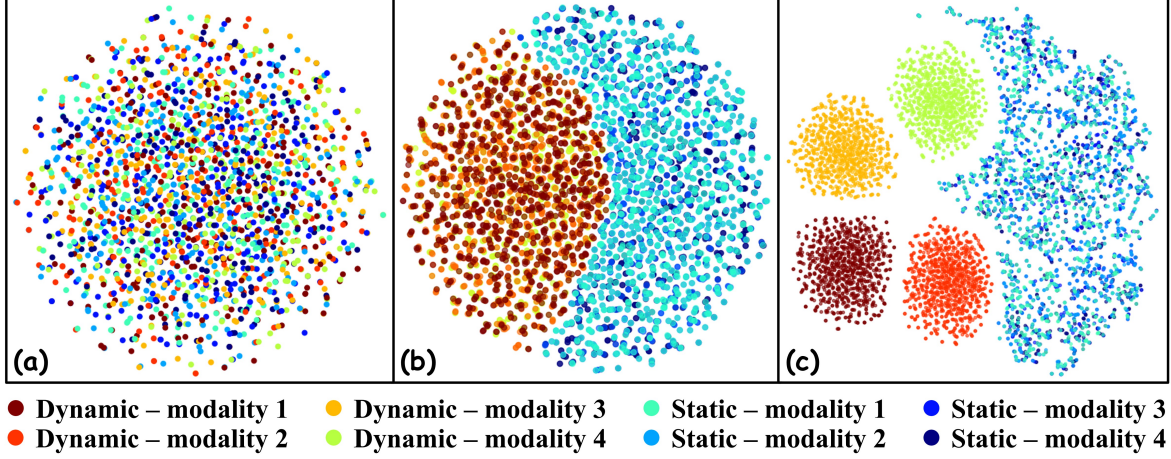


Figure 8: The t-SNE plots of features. (a) Entangled features are inseparable. (b) If we only use two branches to reconstruct the static and dynamic features respectively, the features are separated into two distinct clusters (left - dynamic/right - static). (c) If we further use $\mathcal{L}_{\text{Rank}}$ and \mathcal{L}_{DE} as constraints, the multi-modal dynamic features will also be separated into sub-clusters.

GD-enhancing tumor (ET), peritumoral edema (ED), and the necrotic/non-enhancing tumor core (NCR/NET). Following standard challenge protocols, we evaluated performance on three aggregated regions: Whole Tumor (WT), Tumor Core (TC), and Enhancing Tumor (ET).

4.2 Tasks and Metrics

We designed a comprehensive evaluation protocol covering segmentation, screening, and diagnosis.

Changhai (CH) Dataset:

We implemented a hierarchical pipeline consisting of three tasks: (1) **Tumor Screening**, binary detection of lesion presence; (2) **Benign-Malignant Classification**; and (3) **Subtype Diagnosis**, classification into the four categories described above. Performance for these classification tasks was quantified using the Area Under the Receiver Operating Characteristic Curve (AUC). Additionally, **Tumor Segmentation** performance was evaluated using the Dice Similarity Coefficient.

C4KC-KiTS:

We evaluated **Tumor Segmentation** using Dice, Precision, and Recall. We also assessed **Screening** performance using Accuracy (ACC), Sensitivity (SEN), and AUC.

BraTS 2018:

Consistent with the literature, performance was evaluated solely on **Tumor Segmentation** (WT, TC, ET) using the Dice Similarity Coefficient.

4.3 Implementation Details

We compared TARDIS against four leading methods in incomplete multi-modal learning: RFNet [18], mmFormer [19], M3AE [21], and M²FTrans [20].

All experiments were conducted using PyTorch 1.12 on NVIDIA H20 GPUs. We utilized the AdamW optimizer with a decreasing learning rate schedule initialized at 0.01. The batch size was set to 4, employing the sequence-based optimization strategy detailed in Sec. 3.7. To simulate missing modalities during training, we applied a stochastic modality dropout with a rate of 20%, while ensuring that at least one modality remained available for every training sample. The embedding dictionary size was fixed at 512. The weight β in Eq. 6 was set to 0.25, following [26]. When

training with the BraTS18, the ranking loss $\mathcal{L}_{\text{Rank}}$ was replaced with a separation loss that attempts to push the τ far from each other. All baseline models were retrained and evaluated under identical conditions to ensure fair comparison.

4.4 Comparisons with the State-of-the-Art Methods

We compared TARDiS against four state-of-the-art frameworks designed for incomplete multi-modal segmentation: RFNet, mmFormer, M3AE, and M²FTrans. The quantitative results across the CH, C4KC-KiTS, and BraTS18 datasets are summarized in Tables 1, 2, 3, and 4.

On the large-scale CH dataset, TARDiS consistently outperformed all baselines across both classification and segmentation tasks. As shown in Table 1, our method achieved an average Screening AUC of 0.979, significantly surpassing the second-best method, M²FTrans (0.937). Notably, in the challenging 4-Class Diagnosis task, TARDiS demonstrated remarkable superiority with an AUC of 0.923, whereas competing methods struggled to exceed 0.76. This substantial margin suggests that explicitly disentangling the dynamic tumor enhancement significantly aids in distinguishing subtle histological subtypes.

For segmentation tasks, Table 2 reveals that TARDiS maintains high accuracy even under severe data sparsity. While baseline performance degrades sharply when the arterial or venous phases are missing, TARDiS maintains a robust Dice score of 0.859 on the non-contrast scan alone. This indicates our model’s capability to infer missing hemodynamic information from the learned static anatomy. Similarly, on the public C4KC-KiTS dataset (Table 3), TARDiS achieved the highest scores across all metrics, with a Segmentation Dice of 0.825 and a Screening AUC of 0.965.

Although theoretically grounded in CT hemodynamics, TARDiS generalizes effectively to MRI modalities. As evidenced in Table 4, our framework achieves the highest average Dice scores for Whole Tumor (0.860), Tumor Core (0.759), and the challenging Enhancing Tumor (0.564). Specifically, for the Enhancing Tumor region, which relies heavily on contrast-enhanced sequences, TARDiS outperforms M3AE and RFNet by margins of roughly 12% and 9%, respectively. This confirms that the proposed disentanglement effectively captures temporal-like dependencies between MRI sequences.

All state-of-the-art baselines struggled with the inconvenient design of using separate encoders that require the full set of input modalities to effectively capture the cross-modality information. Their performance severely degrades when facing incomplete inputs. Furthermore, these models, particularly those using transformer-based architectures, often suffer when trained with aggressively large modality dropout rates, which are necessary to simulate clinical sparsity. Our proposed TARDiS architecture, however, addresses this by utilizing a Disentangled Time Attenuated Representation that separates static and dynamic features, enabling robust information inference even when key modalities are missing. This fundamental design difference allows TARDiS to maintain high performance under challenging, sparse training conditions that cause instability in competing methods.

4.5 Modality Ablation and Robustness Analysis

To investigate the impact of different modality combinations and verify the robustness of TARDiS against missing data, we analyzed the performance variations across all possible subsets of inputs, as visualized in Figs. 5 and 6.

In kidney tumor diagnosis, contrast-enhanced phases are clinically critical. Fig. 5 illustrates that baseline methods exhibit jagged performance curves, with deep troughs occurring whenever the ‘A’ or ‘V’ phases are absent. In contrast, TARDiS exhibits a much smoother performance curve. For instance, in the Benign-Malignant classification task, standard methods drop to AUCs below 0.60 when limited to non-contrast data. TARDiS, however, leverages the CVAE-based modal-specific path to hallucinate the missing perfusion features, maintaining an AUC above 0.85 even in the absence of contrast media.

The "missing modality" problem is most severe when only a single modality is available. Table 2 highlights that under the single-modality setting (average of N, A, V, D individual performance), TARDiS achieves an average Dice of roughly 0.86, whereas RFNet and mmFormer lag significantly behind at approximately 0.74 and 0.63, respectively. This robustness is further corroborated by Fig.6 for the BraTS dataset, where the variance in Dice scores across different combinations is visibly lower for TARDiS compared to baselines. This stability implies that our Disentangled Time Attenuated Representation effectively decouples the diagnostic signal from the modality availability, ensuring reliable clinical deployment regardless of the acquisition protocol.

4.6 Qualitative Analysis and Visualization

To intuitively understand the efficacy of TARDiS, we present qualitative segmentation results under the most challenging scenario where only a single modality is available (Fig. 7). In these cases, standard missing-modality frameworks such

as RFNet, mmFormer, and M3AE struggle significantly. As observed in the visual comparisons, these baseline methods often produce fragmented segmentations or fail to detect the tumor entirely, particularly when the highly informative contrast-enhanced phases (arterial or venous) are absent. This failure likely stems from their reliance on channel fusion or masking strategies; when a specific channel is missing, the corresponding diagnostic signal is effectively lost, and the model cannot compensate for the missing hemodynamic information. In contrast, TARDiS maintains high structural consistency with the ground truth across all single-modality inputs. By leveraging the CVAE-based modal-specific path, our model effectively hallucinates the missing perfusion features conditioned on the available static anatomy and the inferred relative time. This capability ensures that the diagnostic boundaries remain distinct even in non-contrast scans, demonstrating the robustness of our generative approach against extreme data sparsity.

We further validate the quality of the learned representations through t-SNE visualization of the latent feature space in Fig. 8. Fig. 8(a) illustrates that without specific disentanglement mechanisms, the feature distributions are entangled, making it difficult to distinguish between anatomical and physiological variations. However, by employing our proposed dual-path architecture, a clear separation emerges between the static and dynamic components, as shown in Fig 8(b). Furthermore, the incorporation of the ranking and disentanglement objectives ($\mathcal{L}_{\text{Rank}}$ and \mathcal{L}_{DE}) refines the dynamic latent space, organizing the features into distinct sub-clusters that correspond to different contrast phases (Fig 8(c)). This structured latent space confirms that TARDiS successfully decouples the time-invariant anatomical information from the time-dependent hemodynamic variations, verifying that the model has learned a physically grounded representation rather than simply memorizing statistical correlations.

5 Conclusion

In this paper, we presented TARDiS, a unified framework for incomplete multi-modal tumor segmentation and classification that moves beyond standard channel-masking strategies. By grounding our architectural design in the physical principles of CT hemodynamics, we hypothesized that the diagnostic signal is composed of a static anatomical baseline and a dynamic perfusion process. The integration of a dictionary-based anatomical encoder ensures structural consistency across scans, while the time-conditioned CVAE allows for the probabilistic reconstruction of dynamic features, even when specific contrast phases are physically absent. Our comprehensive evaluation across large-scale CT and MRI datasets confirms that this physics-aware approach yields superior generalization compared to existing methods that treat modalities as uncorrelated inputs. Specifically, the qualitative and quantitative improvements observed in single-modality inference scenarios suggest that TARDiS can effectively infer missing hemodynamic information from learned latent priors, which validates our hypothesis. Clinically, this work suggests a pathway toward more flexible acquisition protocols. Future work will explore extending this continuous-time modeling to other scenarios like low-dose diagnostic workflows.

References

- [1] Wenya Linda Bi, Ahmed Hosny, Matthew B Schabath, Maryellen L Giger, Nicolai J Birkbak, Alireza Mehrtash, Tavis Allison, Omar Arnaout, Christopher Abbosh, Ian F Dunn, et al. Artificial intelligence in cancer imaging: clinical challenges and applications. *CA: a cancer journal for clinicians*, 69(2):127–157, 2019.
- [2] Kyongtae T Bae. Intravenous contrast medium administration and scan timing at ct: considerations and approaches. *Radiology*, 256(1):32–61, 2010.
- [3] Haseeb Javed, Shaker El-Sappagh, and Tamer Abuhmed. Robustness in deep learning models for medical diagnostics: security and adversarial challenges towards robust ai applications. *Artificial Intelligence Review*, 58(1):12, 2024.
- [4] Qi Dou, Quande Liu, Pheng Ann Heng, and Ben Glocker. Unpaired multi-modal segmentation via knowledge distillation. *IEEE transactions on medical imaging*, 39(7):2415–2425, 2020.
- [5] Cheng Chen, Qi Dou, Yueming Jin, Hao Chen, Jing Qin, and Pheng-Ann Heng. Robust multimodal brain tumor segmentation via feature disentanglement and gated fusion. In *International conference on medical image computing and computer-assisted intervention*, pages 447–456. Springer, 2019.
- [6] Yan Shen and Mingchen Gao. Brain tumor segmentation on mri with missing modalities. In *International conference on information processing in medical imaging*, pages 417–428. Springer, 2019.
- [7] Anmol Sharma and Ghassan Hamarneh. Missing mri pulse sequence synthesis using multi-modal generative adversarial network. *IEEE transactions on medical imaging*, 39(4):1170–1183, 2019.
- [8] Kihyuk Sohn, Honglak Lee, and Xinchen Yan. Learning structured output representation using deep conditional generative models. *Advances in neural information processing systems*, 28, 2015.

- [9] S. Kevin Zhou, Hayit Greenspan, Christos Davatzikos, James S. Duncan, Bram Van Ginneken, Anant Madabhushi, Jerry L. Prince, Daniel Rueckert, and Ronald M. Summers. A review of deep learning in medical imaging: Imaging traits, technology trends, case studies with progress highlights, and future promises. *Proceedings of the IEEE*, 109(5):820–838, 2021.
- [10] Konstantinos Kamnitsas, Christian Ledig, Virginia FJ Newcombe, Joanna P Simpson, Andrew D Kane, David K Menon, Daniel Rueckert, and Ben Glocker. Efficient multi-scale 3d cnn with fully connected crf for accurate brain lesion segmentation. *Medical image analysis*, 36:61–78, 2017.
- [11] Fausto Milletari, Nassir Navab, and Seyed-Ahmad Ahmadi. V-net: Fully convolutional neural networks for volumetric medical image segmentation. In *2016 fourth international conference on 3D vision (3DV)*, pages 565–571. Ieee, 2016.
- [12] Jose Dolz, Karthik Gopinath, Jing Yuan, Herve Lombaert, Christian Desrosiers, and Ismail Ben Ayed. Hyperdense-net: A hyper-densely connected cnn for multi-modal image segmentation. *IEEE transactions on medical imaging*, 38(5):1116–1126, 2018.
- [13] Ali Hatamizadeh, Yucheng Tang, Vishwesh Nath, Dong Yang, Andriy Myronenko, Bennett Landman, Holger R Roth, and Daguang Xu. Unetr: Transformers for 3d medical image segmentation. In *Proceedings of the IEEE/CVF winter conference on applications of computer vision*, pages 574–584, 2022.
- [14] Mohammad Havaei, Nicolas Guizard, Nicolas Chapados, and Yoshua Bengio. Hemis: Hetero-modal image segmentation. In *International conference on medical image computing and computer-assisted intervention*, pages 469–477. Springer, 2016.
- [15] Reuben Dorent, Samuel Joutard, Marc Modat, Sébastien Ourselin, and Tom Vercauteren. Hetero-modal variational encoder-decoder for joint modality completion and segmentation. In *International Conference on Medical Image Computing and Computer-Assisted Intervention*, pages 74–82. Springer, 2019.
- [16] Minhao Hu, Matthis Maillard, Ya Zhang, Tommaso Ciceri, Giammarco La Barbera, Isabelle Bloch, and Pietro Gori. Knowledge distillation from multi-modal to mono-modal segmentation networks. In *International Conference on Medical Image Computing and Computer-Assisted Intervention*, pages 772–781. Springer, 2020.
- [17] Yixin Wang, Yang Zhang, Yang Liu, Zihao Lin, Jiang Tian, Cheng Zhong, Zhongchao Shi, Jianping Fan, and Zhiqiang He. Acn: Adversarial co-training network for brain tumor segmentation with missing modalities. In *International conference on medical image computing and computer-assisted intervention*, pages 410–420. Springer, 2021.
- [18] Yuhang Ding, Xin Yu, and Yi Yang. Rfnnet: Region-aware fusion network for incomplete multi-modal brain tumor segmentation. In *Proceedings of the IEEE/CVF international conference on computer vision*, pages 3975–3984, 2021.
- [19] Yao Zhang, Nanjun He, Jiawei Yang, Yuexiang Li, Dong Wei, Yawen Huang, Yang Zhang, Zhiqiang He, and Yefeng Zheng. mmformer: Multimodal medical transformer for incomplete multimodal learning of brain tumor segmentation. In *International conference on medical image computing and computer-assisted intervention*, pages 107–117. Springer, 2022.
- [20] Junjie Shi, Li Yu, Qimin Cheng, Xin Yang, Kwang-Ting Cheng, and Zengqiang Yan. Mftrans: Modality-masked fusion transformer for incomplete multi-modality brain tumor segmentation. *IEEE Journal of Biomedical and Health Informatics*, 28(1):379–390, 2024.
- [21] Hong Liu, Dong Wei, Donghuan Lu, Jinghan Sun, Liansheng Wang, and Yefeng Zheng. M3ae: Multimodal representation learning for brain tumor segmentation with missing modalities. In *Proceedings of the AAAI conference on artificial intelligence*, volume 37, pages 1657–1665, 2023.
- [22] Xun Huang, Ming-Yu Liu, Serge Belongie, and Jan Kautz. Multimodal unsupervised image-to-image translation. In *Proceedings of the European conference on computer vision (ECCV)*, pages 172–189, 2018.
- [23] Hsin-Ying Lee, Hung-Yu Tseng, Jia-Bin Huang, Maneesh Singh, and Ming-Hsuan Yang. Diverse image-to-image translation via disentangled representations. In *Proceedings of the European conference on computer vision (ECCV)*, pages 35–51, 2018.
- [24] Agisilaos Chartsias, Thomas Joyce, Mario Valerio Giuffrida, and Sotirios A Tsaftaris. Multimodal mr synthesis via modality-invariant latent representation. *IEEE transactions on medical imaging*, 37(3):803–814, 2017.
- [25] Agisilaos Chartsias, Thomas Joyce, Giorgos Papanastasiou, Scott Semple, Michelle Williams, David E Newby, Rohan Dharmakumar, and Sotirios A Tsaftaris. Disentangled representation learning in cardiac image analysis. *Medical image analysis*, 58:101535, 2019.
- [26] Aaron Van Den Oord, Oriol Vinyals, et al. Neural discrete representation learning. *Advances in neural information processing systems*, 30, 2017.

- [27] Tao Zhou, Huazhu Fu, Geng Chen, Jianbing Shen, and Ling Shao. Hi-net: hybrid-fusion network for multi-modal mr image synthesis. *IEEE transactions on medical imaging*, 39(9):2772–2781, 2020.
- [28] Dong Nie, Roger Trullo, Jun Lian, Caroline Petitjean, Su Ruan, Qian Wang, and Dinggang Shen. Medical image synthesis with context-aware generative adversarial networks. In *International conference on medical image computing and computer-assisted intervention*, pages 417–425. Springer, 2017.
- [29] Yilan Zhang, Yingxue Xu, Jianqi Chen, Fengying Xie, and Hao Chen. Prototypical information bottlenecking and disentangling for multimodal cancer survival prediction. In *The Twelfth International Conference on Learning Representations*, 2024.
- [30] Pengyu Cheng, Weituo Hao, Shuyang Dai, Jiachang Liu, Zhe Gan, and Lawrence Carin. Club: A contrastive log-ratio upper bound of mutual information. In *International conference on machine learning*, pages 1779–1788. PMLR, 2020.
- [31] Nicholas Heller, Nihal Sathianathan, Abdul Kalapara, Evan Walczak, Katrina Moore, Heather Kaluzniak, Justin Rosenberg, Phillip Blake, Zack Rengel, Matthew Oestreich, James Dean, Miles Tradewell, Anis Shah, Rushi Tejpaul, Zachary Edgerton, Molly Peterson, Shah Raza, Sujant Regmi, Nicholas Papanikolopoulos, and Christopher Weight. Data from C4KC-KiTS, 2019. Data set.
- [32] Nicholas Heller, Niranjan Sathianathan, Arveen Kalapara, Edward Walczak, Keenan Moore, Heather Kaluzniak, Joel Rosenberg, Paul Blake, Zachary Rengel, Makinna Oestreich, et al. The kits19 challenge data: 300 kidney tumor cases with clinical context, ct semantic segmentations, and surgical outcomes. *arXiv preprint arXiv:1904.00445*, 2019.
- [33] Nicholas Heller, Fabian Isensee, Klaus H Maier-Hein, Xiaoshuai Hou, Chunmei Xie, Fengyi Li, Yang Nan, Guangrui Mu, Zhiyong Lin, Miofei Han, et al. The state of the art in kidney and kidney tumor segmentation in contrast-enhanced ct imaging: Results of the kits19 challenge. *Medical Image Analysis*, page 101821, 2020.
- [34] Bjoern H Menze, Andras Jakab, Stefan Bauer, Jayashree Kalpathy-Cramer, Keyvan Farahani, Justin Kirby, Yuliya Burren, Nicole Porz, Johannes Slotboom, Roland Wiest, et al. The multimodal brain tumor image segmentation benchmark (brats). *IEEE transactions on medical imaging*, 34(10):1993–2024, 2014.
- [35] Spyridon Bakas, Hamed Akbari, Aristeidis Sotiras, Michel Bilello, Martin Rozycki, Justin S Kirby, John B Freymann, Keyvan Farahani, and Christos Davatzikos. Advancing the cancer genome atlas glioma mri collections with expert segmentation labels and radiomic features. *Scientific data*, 4(1):1–13, 2017.
- [36] Spyridon Bakas, Mauricio Reyes, Andras Jakab, Stefan Bauer, Markus Rempfler, Alessandro Crimi, Russell Takeshi Shinohara, Christoph Berger, Sung Min Ha, Martin Rozycki, et al. Identifying the best machine learning algorithms for brain tumor segmentation, progression assessment, and overall survival prediction in the brats challenge. *arXiv preprint arXiv:1811.02629*, 2018.